

International Conference on Industry Sciences and Computer Science Innovation

Single Image Dehazing via Regional Saturation-Value Translation

Le-Anh Tran^a, Daehyun Kwon^b, Dong-Chul Park^{a,*}

^a*Myongji University, 116 Myeongji Street, Yongin, 17058, South Korea*

^b*Soongsil University, 369 Sangdo Street, Seoul, 06978, South Korea*

Abstract

This paper proposes an image dehazing prior, called Regional Saturation-Value Translation (RSVT), in order to address the color distortion issues produced by prevailing prior-based dehazing methods when processing hazy images with large sky regions. The proposed RSVT prior is derived from statistical analyses of the correlation between hazy points and respective haze-free points in the HSV color space. The prior is based upon two key observations in the sky areas. First, the difference in terms of hue for a pair of hazy and haze-free points is very small, raising an assumption that the variability of pixel values caused by haze mostly occurs in the saturation and value spaces. This leads to the second observation that, in the 2D saturation-value coordinate system, almost all the lines passing through corresponding pairs of hazy-clean points, termed S-V lines, are likely to intersect around the airlight coordinates. A hybrid refined dark channel is introduced in order to decompose the input hazy image into sky and non-sky regions and to estimate the global atmospheric light. Combining the prior with the hybrid refined dark channel, a novel single image dehazing framework is proposed. Haze removal is performed separately for the sky and non-sky regions by adopting the proposed RSVT prior and Koschnieder's law, respectively. The experimental results have shown that the proposed dehazing method can restore visually compelling sky color and effectively handle the color distortion issues associated with large sky regions.

© 2022 The Authors. Published by Elsevier B.V.

This is an open access article under the CC BY-NC-ND license (<http://creativecommons.org/licenses/by-nc-nd/4.0/>)

Peer-review under responsibility of the scientific committee of the International Conference on Industry Sciences and Computer Sciences Innovation.

Keywords: Image dehazing; image defogging; haze removal; image restoration; dehazing prior.

1. Introduction

The natural atmosphere always contains turbid mediums such as water droplets and particles, which present strong absorption and scattering of light during the propagation process, resulting in the attenuation of the scene radiance along the line of sight. Such phenomena are haze and fog that can be easily observed in digital images captured from outdoor scenes. As a result, the scene radiance received by the camera is degraded leading to the production of low-quality outdoor images with a loss in contrast and low color fidelity. Since the scene radiance decreases and the airlight magnitude increases, a hazy image can be modeled as a per-pixel convex combination between the actual

* Corresponding author.

E-mail address: parkd@mju.ac.kr

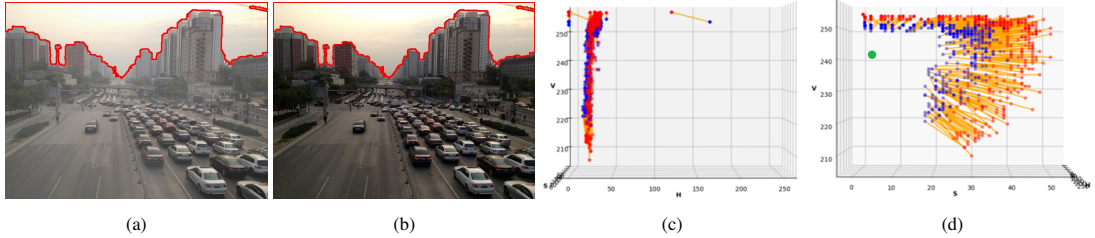


Fig. 1: Regional Saturation-Value Transition: (a) and (b) are hazy and clean images, respectively, with the sky regions marked in red boundaries; (c) and (d) display hazy (blue) and clean (red) points for the sky region in HSV color space from Hue-Value and Saturation-Value perspectives, respectively (orange segments connect corresponding hazy-clean pairs).

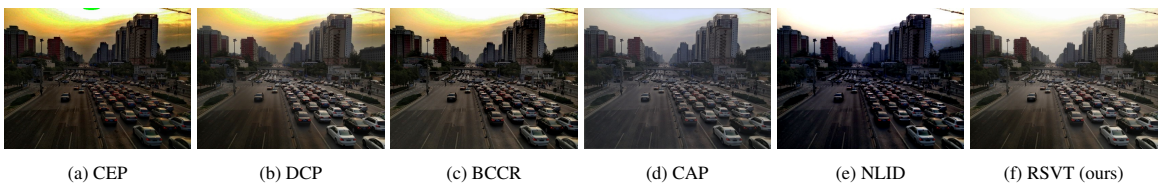


Fig. 2: Dehazing results of various prior-based approaches on the hazy image in Fig. 1a: (a) CEP [2], (b) DCP [3], (c) BCCR [8], (d) CAP [15], (e) NLID [1], and (f) the proposed RSVT framework.

scene radiance and the global atmospheric light [1], this model is known as the scattering atmospheric model or Koschmieder's law [9]:

$$I(x) = J(x)t(x) + A(1 - t(x)), \quad (1)$$

where $I(x)$, $J(x)$, A , and $t(x)$ denote the observed intensity, the scene radiance, the global atmospheric light, and the transmission map, respectively. When the atmospheric light is homogenous, $t(x)$ can be expressed as [3, 12, 13]:

$$t(x) = e^{-\beta d(x)}, \quad (2)$$

where β represents the scattering coefficient of the atmosphere and $d(x)$ denotes the scene depth.

Low-quality images can lead to the deprivation of human and machine vision, introducing a negative effect on real-world vision-based applications such as object detection or autonomous driving systems [11], therefore, haze removal is highly desired. As an ill-posed challenging problem, image dehazing has attracted a great number of research and made significant progress. Generally, haze removal algorithms can be categorized into two groups: prior-based and deep learning-based methods. Each genre has its own advantages and disadvantages. Prior-based methods are preferable for restoring visibility while deep learning-based approaches can be applied to improve the realism [14]. However, prior-based algorithms usually suffer over-saturation and leave artifacts in the outputs, whereas learning-based models are highly dependent on large training datasets which are an expensive issue for dehazing tasks.

In this paper, we propose a new prior, called *Regional Saturation-Value Translation* (RSVT), in order to overcome the drawbacks of prevailing prior-based dehazing methods. The prior is based on two key observations in the sky and large homogeneous hazy areas of hazy-clean image pairs. First, the difference in terms of hue for a pair of hazy and haze-free points is very small, as shown in Fig. 1c, and it raises an assumption that the effect of haze on the hue channel is trivial. This leads to the second observation: given the 2D coordinate system formed by the saturation and value channels of the HSV color space, most of the lines passing through corresponding pairs of hazy-clean points, termed *S-V lines*, are likely to intersect around the airlight, as can be noticed in Fig. 1d. Based on these observations, the haze-free pixel can be estimated by translating the hazy point by a proper amount in the S-V coordinate system. Our proposed prior is based on various statistical analyses. The proposed prior is independent of the scattering atmospheric model and does not require a training process. We find that our proposed prior is very robust and effective for large homogeneous hazy regions. Interestingly, dehazing quality of the sky and/or large homogeneous hazy areas has been one of the main drawbacks of the classical dark channel prior (DCP) [3] and some other prevailing dehazing priors.

As can be seen in Fig. 2a-2e, various prior-based methods give favorable results in the non-sky regions but suffer color distortion in the sky regions. Combing our proposed prior with DCP, we introduce a robust and effective haze removal framework. A typical dehazing result obtained by our proposed dehazing method is shown in Fig. 2f. Note that our proposed method can reduce much of the color distortion in the sky regions and recover a visually compelling dehazed image compared to other prevailing algorithms.

The remainder of this paper is organized as follows: Section 2 provides a brief review of single image dehazing. Several assumptions along with statistical analyses in order to verify the prior are presented in Section 3. Combining the proposed prior with DCP, a new single image dehazing framework is proposed in Section 4. Section 5 discusses the experimental results and Section 6 concludes the paper.

2. Brief Review on Image Dehazing

As mentioned in Section 1, haze removal algorithms can be categorized into two groups: prior-based and deep learning-based methods.

The prior-based methods mostly rely on the scattering atmospheric model to perform haze-free image recovery. That is, from Eq. (1), the estimation of actual scene radiance $\hat{J}(x)$ is expressed as:

$$\hat{J}(x) = \frac{I(x) - A(1 - t(x))}{\max(t_0, t(x))}, \quad (3)$$

where t_0 is a lower bound of $t(x)$ to preserve a small amount of haze in extremely dense haze-opaque regions and to avoid dividing by zero. Relying on this recovering function, dehazed image can be obtained by solving the unknowns $t(x)$ and A . Meng *et al.* [8] proposed an efficient method that enforces the boundary constraint and contextual regularization (BCCR) for sharper dehazed images. Zhu *et al.* [15] proposed a color-attenuation prior (CAP) that models the scene depth of a hazy image and learns the parameters of the model through a supervised learning method. Berman *et al.* [1] introduced a non-local image dehazing (NLID) prior based on an observation that the hazy pixels in RGB color space are distributed along lines passing through the airlight. Among prior-based methods, dark channel prior (DCP) [3] has been the most attractive method. DCP is developed based on an observation that most local patches in haze-free outdoor images contain some pixels with very low intensity in at least one color channel. The DCP method can effectively estimate the haze thickness and the haze-free image is recovered via Eq. (3).

In contrast to prior-based approaches, learning-based algorithms can learn to estimate A , $t(x)$, or $\hat{J}(x)$ directly from the input hazy image [6, 14]. Convolution neural networks (CNNs) are usually adopted as the main backbones of those learning-based methods that can produce impressive dehazing results. However, the training process of CNNs requires large training datasets with pairs of hazy and haze-free images from the same scenes, which are too difficult and/or unachievable to prepare under real-world circumstances. A common solution to this issue is to utilize synthetic hazy images, but there always exists a certain gap between the synthetic and real-world data. In addition, learning-based models usually overfit the synthetic training data and their generalization ability to realistic haze is insufficient.

Even though learning-based approaches are dominant in the current deep learning era, we believe that developing novel prior-based models is also important. In the next section, we present a new prior which can be combined with DCP to form a unified haze removal framework that can restore high-quality haze-free images.

3. Regional Saturation-Value Variability

The proposed prior is based on two principal observations in the sky areas of hazy-clean image pairs. First, the effect of haze on the hue channel is trivial, and second, in the 2D saturation-value coordinate system, almost all the S-V lines are likely to intersect around the airlight coordinates. In order to verify the above observations, we have selected 1,000 hazy-clean image pairs from the RESIDE Outdoor dataset [7] which contain sky regions and then conducted various statistical analyses. The sky regions were extracted by applying a hybrid refined dark channel (described in Section 4.1) and manual checking. From these efforts, the following three assumptions have been created and tested for the validation of the proposed prior.

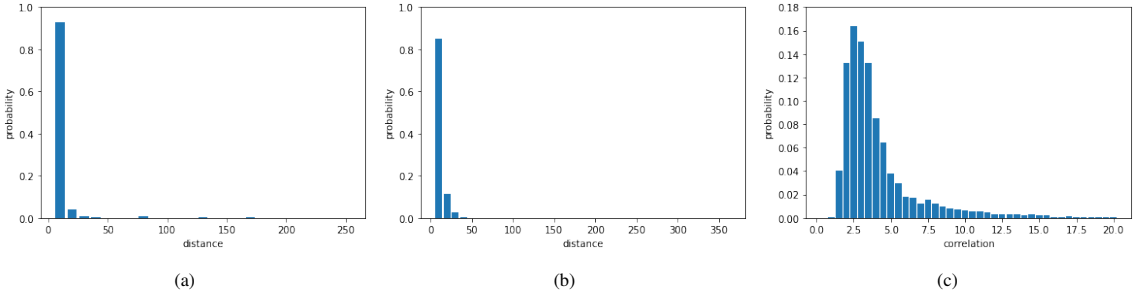


Fig. 3: Statistical analyses: (a) Differences between the hue components of hazy and haze-free point pairs within the sky regions (each bin stands for 10 distance levels), (b) Distances between the intersections of S-V lines and the global atmospheric light coordinates in the Saturation-Value coordinate system (each bin stands for 10 distance levels), and (c) Distribution of the correlation between the S-V ratio and the transmission.

3.1. The 1st Assumption

The first assumption states that: for the sky regions, the hue component of one pixel in a hazy image and that of the corresponding pixel in the haze-free image are relatively identical, as can be noticed in Fig. 1c. Based on this observation, dehazing for the sky regions can be carried out without considering the hue space because the variability of pixel values mostly occurs in the saturation and value spaces, as can be noticed in Fig. 1d.

To verify this assumption, the absolute differences between the hue components of hazy and haze-free point pairs within the sky areas are measured and a probability distribution as shown in Fig. 3a is obtained. As can be seen from Fig. 3a, around 93% of the distances are lower than 10 which verifies our first assumption.

3.2. The 2nd Assumption

The second assumption states that: by assuming that the haze distribution in the sky regions is homogeneous, we have observed that almost all the S-V lines are likely to intersect around a location that is very close to the atmospheric light coordinates because the atmospheric light is usually fallen within the sky area of a hazy image.

To verify the second assumption, for each hazy-clean image pair, we computed the intersection E of all the S-V lines and measured the Euclidean distance between E and the global atmospheric light A which is estimated by randomly applying DCP [3] and NLID [1]:

$$\|E - A\| = \sqrt{(S_E - S_A)^2 + (V_E - V_A)^2}, \quad (4)$$

where S and V are saturation and value components, respectively. Note that $S, V \in [0, 255]$, thus the maximum distance is $\sqrt{255^2 + 255^2} \approx 360$. Note also that all the S-V lines do not intersect perfectly at one single point, hence, we collected every intersection of each pair of S-V lines, and E was computed as the average of all the intersections. Fig. 3b shows the distances between the S-V lines' intersections and the global atmospheric light coordinates of 1,000 hazy-clean image pairs. As can be seen in Fig. 3b, almost all distances are close to small values, which suggests that the intersection is usually close to the atmospheric light. This statistic gives very strong support to the third assumption.

3.3. The 3rd Assumption

From Fig. 1d, we have observed that, each clean point $c(x)$ is obtained by translating the respective hazy point $h(x)$ far away from the intersection E (marked as a green point) by an amount that is directly proportional to the distance from the hazy point to the intersection, $\|h(x) - E\|$. The problem now is to find the relation between $\|h(x) - E\|$ and any information possibly related to the haze distribution in the input hazy image. Interestingly, in the haze imaging model, the transmission in the RGB color space is expressed as [3]:

$$t(x) = \frac{\|I(x) - A\|}{\|J(x) - A\|}, \quad (5)$$

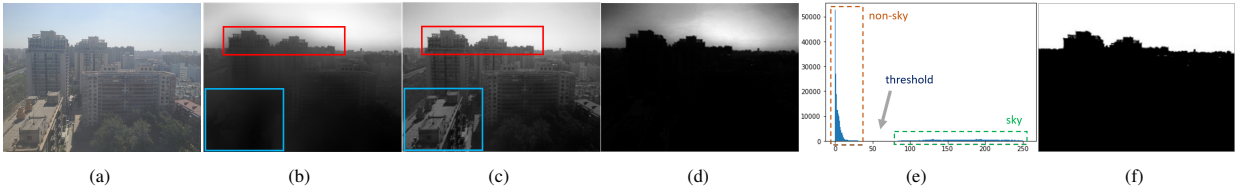


Fig. 4: Hybrid refined dark channel: (a) Hazy image, (b) Refined dark channel with $W = 30$, (c) Refined dark channel with $W = 3$, (d, e) Hybrid refined dark channel and its histogram, (f) Extracted sky mask with a threshold of 50.

which implies that the ratio between the distance from the hazy point to the airlight and the distance from the haze-free point to the airlight in RGB color space directly represents the transmission. This leads us to the investigation of a similar kind of ratio in HSV color space. To this end, we first omitted two types of lines: one is the S-V lines whose hazy or clean points have the value or saturation component close to 0 or 255 since these points' magnitudes may be trimmed due to the 8-bit image property, and the other type includes too short lines which may be deemed as “outliers” when calculating the ratio distribution. Then we computed a component termed S-V ratio, parameterized as $r(x)$, for each S-V line:

$$r(x) = \frac{\|h(x) - E\|}{\|c(x) - E\|}, \quad (6)$$

and we examined the distribution of $R(x)$ which denotes the correlation between S-V ratio and transmission:

$$R(x) = \frac{r(x)}{t_s(x)}, \quad (7)$$

where $t_s(x)$ denotes the transmission of the sky regions. To compute $t_s(x)$, we have referred to the method described in [5] which utilizes the dark channel with small window size (3×3) to estimate proper transmission in the sky regions:

$$t_s(x) = 1 - \omega \min_{y \in p_{3 \times 3}(x)} \left(\min_{c \in (r,g,b)} \frac{I_c(y)}{A_c} \right), \quad (8)$$

where ω ($0 < \omega \leq 1$) is typically set to 0.95 to optionally keep a small amount of haze for distant objects [3]. Fig. 3c shows the obtained distribution of $R(x)$, we roughly assume that $R(x)$ for any image can be set as a constant such that the restored image's intensities will not be affected significantly when the value of $R(x)$ varies in a narrow range. In fact, $R(x)$ can be fine-tuned for each image in order to obtain an optimal result.

4. The Proposed Dehazing Method

4.1. Hybrid Refined Dark Channel

In Fig. 4b, a dark channel with a large window size ($W = 30$) can process a large local region and, therefore, there is a high probability of finding the pixels with low intensity which commonly belong to objects in the non-sky regions, as can be noticed from the blue box; at the same time, shadow artifacts are created around the edge regions after post-processing by applying guided filtering [4], as can be noticed from the red box. On the other hand, in Fig. 4c, a dark channel with a small window size ($W = 3$) can find the dark pixels in a small region which can leave the sky regions brighter at the edges, as can be seen from the red box, however, it can not fill the regions of the bright objects, as can be seen from the blue box, and that may lead to color distortion in the final restored image. Note that the dark channels shown in Fig. 4b and 4c are refined by performing guided filtering [4]. In order to effectively extract the sky regions by combining the merits of both types of dark channels, we compute a hybrid refined dark channel d_H :

$$d_H = (d_L)^a * (d_S)^b, \quad (9)$$

where d_L and d_S are the refined dark channels with large and small window sizes, respectively, while a and b are the power weight coefficients. By the effect of the power weights, the intensities of the non-sky regions become very

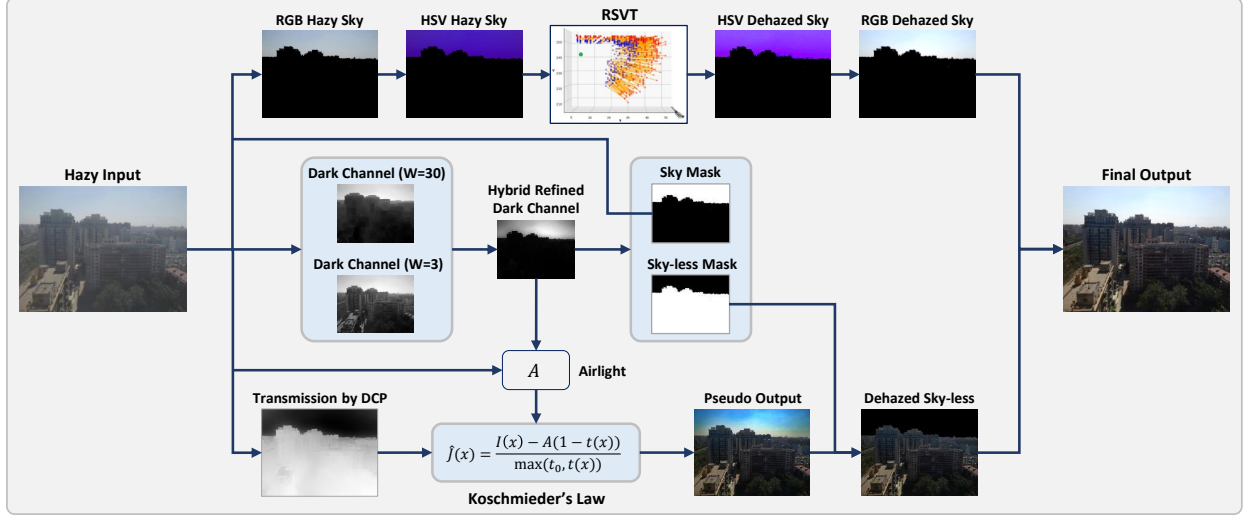


Fig. 5: The proposed RSVT dehazing framework.

low (close to zero). Fig. 4d and 4e show a hybrid refined dark channel (with $a = 1$ and $b = 4$) and its histogram, respectively. As can be noticed in Fig. 4e, the sky and non-sky pixels are effectively segregated, and the sky mask can be obtained by adopting binary segmentation with the threshold chosen as the pixel value having the lowest frequency within the pixel range of (10, 100) in the histogram. Fig. 4f shows an extracted sky mask with a threshold of 50.

4.2. Atmospheric Light Estimation

The traditional DCP estimates the airlight by picking the pixels with the highest intensity respective to the top 0.1% brightest pixels in the dark channel [3], but this method may be ineffective when there is a presence of bright/white objects, since the regions of white objects may be selected to be the airlight. In order to have a better selection of global atmospheric light, we refer to the top 0.1% brightest pixels in the hybrid refined dark channel as it is able to get rid of the bright regions which may belong to the bright/white objects, this effect can be seen in Fig. 4d as an example.

4.3. Regional Saturation-Value Translation

As mentioned in Section 3.3, when the atmospheric light is obtained, the haze-free point can be estimated by translating the hazy point far away from the atmospheric light by an amount directly proportional to its distance to the atmospheric light. Now we have to determine the amount of translation in order to estimate the haze-free point.

Based on the distribution of $R(x)$ shown in Fig. 3c, we assume that $R(x)$ can be set as a constant for any image such that the intensities of the restored image are not affected considerably when the value of $R(x)$ varies in a small range. Note that $R(x)$ can be fine-tuned for each image in order to obtain an optimal result. From this assumption, we typically set $R(x) = 3$. From Eq. (6) we have:

$$\frac{\|c(x) - A\|}{\|h(x) - A\|} = \frac{1}{r(x)}. \quad (10)$$

Note that the intersection E is replaced with the estimated airlight A based on the proven assumption in Section 3.2. From Eq. (7), the above equation is equivalent to:

$$\frac{\|c(x) - h(x)\|}{\|h(x) - A\|} + 1 = \frac{1}{R(x)t_s(x)}. \quad (11)$$

The translation quantity now can be calculated as:

$$\|c(x) - h(x)\| = \frac{1 - R(x)t_s(x)}{R(x)t_s(x)}\|h(x) - A\|. \quad (12)$$

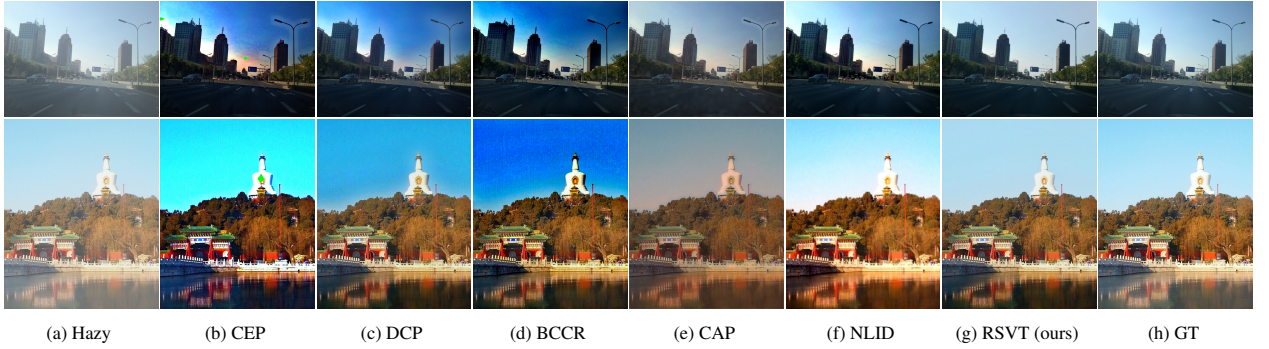


Fig. 6: Typical results of various approaches on SOTS Outdoor dataset.

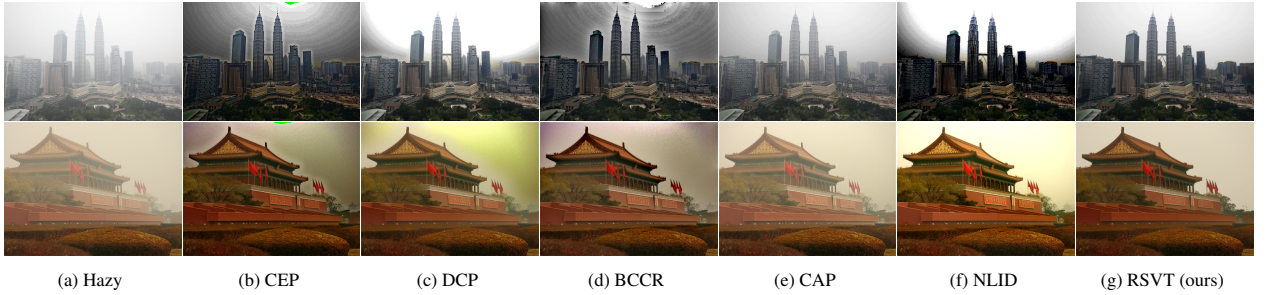


Fig. 7: Typical results of various approaches on natural hazy images.

4.4. Haze-free Image Recovery

Eventually, dehazing is performed separately for the sky and non-sky regions by adopting the proposed saturation-value translation prior and Koschmieder's law, respectively. The proposed dehazing model is formulated as follows:

$$J(x) = \frac{I(x) - A(1 - t(x))}{\max(t_0, t(x))}(1 - M(x)) + S(x)M(x), \quad (13)$$

where $M(x)$ is the sky mask extracted by adopting the proposed hybrid refined dark channel and $S(x)$ is the dehazed sky regions. Note that when the sky regions are not present, our method works in a similar spirit to DCP with an improved atmospheric light estimation. The diagram of the proposed dehazing framework is illustrated in Fig. 5.

5. Experiments and Discussions

The proposed method is quantitatively and qualitatively compared to other prevailing prior-based approaches including CEP [2], FVR [10], DCP [3], CAP [15], NLID [1], and BCCR [8]. The comparisons were conducted on SOTS Outdoor dataset [7] and several real-world hazy images. We set $a = 1$ and $b = 4$ in our experiments. The quantitative results were measured using Peak Signal-to-Noise Ratio (PSNR) and Structural Similarity Index Measure (SSIM).

5.1. Quantitative Evaluations

Table 1 summarizes the quantitative performances of various prior-based dehazing approaches on the SOTS Outdoor dataset. As summarized in Table 1, the proposed dehazing framework outperforms all the other approaches in terms of both PSNR and SSIM metrics, especially, the SSIM produced by the proposed method (0.8918) is considered much better than those given by the other algorithms. The proposed dehazing framework processes a 550x410 image in around 0.32s with an Intel(R) Core(TM) i5-8600K CPU @ 3.60GHz.

Method	CEP [2]	FVR [10]	DCP [3]	BCCR [8]	NLID [1]	CAP [15]	RSVT (ours)
PSNR	13.44	15.72	16.62	16.88	17.29	19.05	20.33
SSIM	0.7053	0.7483	0.8179	0.7913	0.7489	0.8364	0.8918

Table 1: Quantitative performances of various dehazing methods on SOTS Outdoor dataset.

5.2. Qualitative Evaluations

Typical visual dehazing results of different methods on SOTS Outdoor dataset are shown in Fig. 6. As can be seen from Fig. 6, the proposed method can produce visually compelling dehazed images when compared to other prior-based methods. Note that the appearance of the sky regions produced by the proposed RSVT method is significantly improved over those produced by the other approaches. In addition, several visual performance comparisons on natural hazy images are also presented in Fig. 7, which further verify the effectiveness of our method in real-world scenarios. Consequently, we have validated that the proposed prior can address the color distortion problem in the sky regions which is the issue of almost all other prior-based dehazing algorithms.

6. Conclusions

In this paper, a Regional Saturation-Value Transition (RSVT) prior for image dehazing is proposed. The prior is derived from two observations in the sky areas. First, the difference in hue components for a pair of hazy and haze-free points is trivial. Second, in the 2D coordinate system formed by the saturation and value components, almost all the lines passing through corresponding pairs of hazy-clean points are likely to intersect around the airlight coordinates, and haze removal can be performed by translating hazy points by proper amounts. This prior is combined with dark channel prior to introduce a new dehazing framework. In addition, a hybrid refined dark channel is proposed for image decomposition and airlight estimation. The experimental results have demonstrated that the proposed dehazing method can perform effectively and efficiently on hazy scenes with the appearance of sky regions.

References

- [1] Berman, D., Avidan, S., et al., 2016. Non-local image dehazing, in: Proceedings of the IEEE conference on computer vision and pattern recognition, pp. 1674–1682.
- [2] Bui, T.M., Kim, W., 2017. Single image dehazing using color ellipsoid prior. *IEEE Transactions on Image Processing* 27, 999–1009.
- [3] He, K., Sun, J., Tang, X., 2010. Single image haze removal using dark channel prior. *IEEE transactions on pattern analysis and machine intelligence* 33, 2341–2353.
- [4] He, K., Sun, J., Tang, X., 2012. Guided image filtering. *IEEE transactions on pattern analysis and machine intelligence* 35, 1397–1409.
- [5] Huang, S.C., Jaw, D.W., Li, W., Lu, Z., Kuo, S.Y., Fung, B.C., Chen, B.H., Numnonda, T., 2021. Image dehazing in disproportionate haze distributions. *IEEE Access* 9, 44599–44609.
- [6] Li, B., Peng, X., Wang, Z., Xu, J., Feng, D., 2017. Aod-net: All-in-one dehazing network, in: Proceedings of the IEEE international conference on computer vision, pp. 4770–4778.
- [7] Li, B., Ren, W., Fu, D., Tao, D., Feng, D., Zeng, W., Wang, Z., 2018. Benchmarking single-image dehazing and beyond. *IEEE Transactions on Image Processing* 28, 492–505.
- [8] Meng, G., Wang, Y., Duan, J., Xiang, S., Pan, C., 2013. Efficient image dehazing with boundary constraint and contextual regularization, in: Proceedings of the IEEE international conference on computer vision, pp. 617–624.
- [9] Middleton, W., Twersky, V., 1954. Vision through the atmosphere. *Physics Today* 7, 21.
- [10] Tarel, J.P., Hautiere, N., 2009. Fast visibility restoration from a single color or gray level image, in: 2009 IEEE 12th international conference on computer vision, IEEE. pp. 2201–2208.
- [11] Tran, L.A., Le, M.H., 2019. Robust u-net-based road lane markings detection for autonomous driving, in: 2019 International Conference on System Science and Engineering (ICSSE), IEEE. pp. 62–66.
- [12] Tran, L.A., Moon, S., Park, D.C., 2022. A novel encoder-decoder network with guided transmission map for single image dehazing. *Procedia Computer Science* 204, 682–689.
- [13] Tran, L.A., Park, D.C., 2022. Encoder-decoder network with guided transmission map: Robustness and applicability, in: International Symposium on Intelligent Informatics, Springer. pp. 41–54.
- [14] Zhao, S., Zhang, L., Shen, Y., Zhou, Y., 2021. Refinednet: A weakly supervised refinement framework for single image dehazing. *IEEE Transactions on Image Processing* 30, 3391–3404.
- [15] Zhu, Q., Mai, J., Shao, L., 2015. A fast single image haze removal algorithm using color attenuation prior. *IEEE transactions on image processing* 24, 3522–3533.